



Automatic lung cancer detection from CT image using optimized Robust Deformed Convolutional Neural Network with TriHorn-Net

C Lokanath Reddy ^{a,b,*}, M.V.D. Prasad ^c

^a Research Scholar, Electronics and Communication Engineering, Koneru Lakshmaiah Education Foundation, Vaddeswaram, Andhra Pradesh, India

^b Assistant Professor, Electronics and Communication Engineering, G. Pullaiah College of Engineering and Technology, Kurnool, Andhra Pradesh, India

^c Associate Professor, Electronics and Communication Engineering, Koneru Lakshmaiah Education Foundation, Vaddeswaram, Andhra Pradesh, India



ARTICLE INFO

Keywords:

Automatically Weighted Binary Multi-View Clustering
Robust Deformed Convolutional Neural Network
Second-Order Synchroextracting Wavelet Transform
Sub Aperture Keystone Transform Matched Filtering
TriHorn-Net
Wader Hunt Optimization Algorithm

ABSTRACT

Lung cancer is a leading cause of death for both men and women, requires accurate and early detection to improve treatment outcomes. The inability of traditional approach to handle intricate nodule formations, subpar segmentation methods, and low-quality CT images results in inaccurate predictions. To overcome these complications, Automatic Lung Cancer Detection from CT image using optimized Robust Deformed Convolutional Neural Network with TriHorn-Net (RDCNN-TriHorn-Net-WHOA-ALCD) is proposed. The input CT images, sourced from the Chest CT-Scan Images Dataset and Formatted and Augmented Chest CT-Scan images dataset, undergo preprocessing via Sub Aperture Keystone Transform Matched Filtering (SAKTMF) to reduce noise and improve image quality. Automatically Weighted Binary Multi-View Clustering (AW-BMVC) is used to segment the affected regions, and the Second-Order Synchroextracting Wavelet Transform (SOSWT) is used to extract spectral features. Classification is conducted using Robust Deformed Convolutional Neural Network (RDCNN) models across three strategies. In Strategy 1, RDCNN-TriHorn-Net with Wader Hunt Optimization Algorithm (WHOA) outperformed other models in detecting lung cancer. In Strategy 2 showed RDCNN-ResNeXt-50 with Adaptive Elite Ant Lion Optimization Algorithm (AEALOA) yielded better results, while Strategy 3 highlighted RDCNN-CoAtNet with Dipper Throated Optimization Algorithm (DTOA). The RDCNN-TriHorn-Net-WHOA-ALCD method achieved superior classification of lung CT images, like Large Cell Carcinoma (LCC), Adenocarcinoma, Normal, and Squamous Cell Carcinoma (SCC) in the Chest CT-Scan images dataset, as well as normal and Squamous in the Formatted and Augmented Chest CT-Scan images dataset. The proposed RDCNN-TriHorn-Net-WHOA-ALCD technique is implemented in Python. The effectiveness of the RDCNN-TriHorn-Net-WHOA-ALCD approach attains 13.67%, 27.55% and 14.67 dice similarity coefficient and 22.23%, 24.11% and 25.56% logarithmic loss compared with existing techniques respectively.

1. Introduction

The majority of individuals in developing technologies suffer from genetic problems (Nissar and Mir, 2024) as a result of erroneous mutations that fundamentally alter human lifestyles (Wani et al., 2024; Zhang et al., 2024; Venkatesan et al., 2024). Lung cancer is a prevalent illness in the medical field to be diagnosed at an earlier stage, according

to the data (Lin et al., 2024; Imran et al., 2024). The symptoms of lung cancer, such as blood in the cough, chest pain, breath shortness, exhaustion, weight and memory loss, bone fracture, joint pain, head ache, nerve issue, haemorrhage, voice change, sputum colour change are typically utilized to predict the disease manually (Kumar et al., 2024; Barbouchi et al., 2023). Various screening approaches (Ashwini et al., 2024), blood tests, fluid biopsies, reflex tests, bronchial scopes, and

Abbreviations: CT, Computed Tomography; SNN, Stacked Neural Network; CNN, Convolutional Neural Network; CSViT-IMFO, Cross Spectral Visual Transformer along Improved Moth Flame Optimisation; DNN, Deep Neural Network; TL, Transfer Learning; SAKTMF, Sub Aperture Keystone Transform Matched Filtering; AW-BMVC, Automatically Weighted Binary Multi-View Clustering; SOSWT, Second-Order Synchroextracting Wavelet Transform; RDCNN, Robust Deformed Convolutional Neural Network; WHOA, Wader Hunt Optimization Algorithm; AEALOA, Adaptive Elite Ant Lion Optimization Algorithm; DTOA, Dipper Throated Optimization Algorithm; TP TN FP FN, True Positive, True Negative, False Positive, False Negative; MAE, Mean Absolute Error (MAE); SS, Sum of Square; DF, Degree of Freedom; MS, Mean Square.

* Corresponding author.

E-mail addresses: chikalalokanathreddy@gmail.com (C. Lokanath Reddy), mvd_ece@kluniversity.in (M.V.D. Prasad).

<https://doi.org/10.1016/j.eswa.2025.127124>

Received 19 December 2024; Received in revised form 3 February 2025; Accepted 1 March 2025

Available online 3 March 2025

0957-4174/© 2025 Elsevier Ltd. All rights are reserved, including those for text and data mining, AI training, and similar technologies.

genetic testing, among others, have been used consistently for evaluation following the patient's exposure to these technologies (Murthy and Prasad, 2023; An et al., 2024; Prasad et al., 2024). The screening techniques that have been presented effectively look at lung cells and cell abnormalities that are employed to forecast lung cancer, but maintaining prediction accuracy is challenging (Wani et al., 2024; Sangeetha et al., 2024; Suganthy et al., 2024). Compared to the positron emission tomography and magnetic resonance imaging screening procedures, the 30-minute X-ray passes successfully check internal organ function and efficiently gather facts about tissues and damaged parts (Priyadarshini et al., 2024; Shao et al., 2024). An automatic lung cancer prediction (Chung et al., 2024; Yoo et al., 2024) system is developed using CT images to identify the disease using a number of conventional techniques, including Cancer classification, image noise reduction, feature selection, region segmentation, and cancer feature extraction (Subash and Kalaivani, 2024).

Improving survival rates from lung cancer requires early detection, but existing detection methods frequently fall short because of issues like poor CT image quality, ineffective segmentation methods, and insufficient classification models (Nagarathna & Chinnaswamy, 2014; Nagarathna & Kusuma, 2021, 2022). In the end, these restrictions cause delayed diagnosis and treatment due to low accuracy, increased false positives, and false negatives. The trustworthiness of current approaches in clinical contexts is further hampered by their generally subpar performance, which includes low Dice similarity coefficients and substantial logarithmic loss.

To overcome these challenges, the RDCNN-TriHorn-Net-WHOA-ALCD uses novel techniques to create a reliable, automated system that can precisely recognize lung cancer in its initial stages from computed tomography scan images. These motivate us to do this work.

Research Questions:

RQ1: which databases are employed in lung cancer diagnosis?

RQ2: which performance matrices are applied for the lung cancer identification to analyse the system?

RQ3: what are the current challenges and limits of the existing studies and the scope of potential future research for lung cancer identification?

The novelty of the Automatic Lung Cancer Detection method using Robust Deformed Convolutional Neural Network with TriHorn-Net optimized by the Wader Hunt Optimization Algorithm lies in its ability to enhance lung cancer detection by addressing challenges like intricate nodule formations and low-quality CT images. The integration of RDCNN with TriHorn-Net allows for improved feature extraction, while the optimization by WHOA ensures efficient model training, leading to superior classification accuracy and robustness compared to traditional methods.

Early lung cancer detection using RDCNN-TriHornNet-WHOA-ALCD. Preprocessing via SAKTMF enhances CT image quality and noise removal. AW-BMVC segments affected regions; SOSWT extracts spectral features. Three RDCNN strategies optimize classification across CT datasets. Achieves superior accuracy, outperforming existing detection methods.

The primary contributions of this paper are deliberated here,

- In this manuscript, RDCNN-TriHorn-Net-WHOA-ALCD is proposed. The method effectively eliminates noise and develops image quality by pre-processing lung CT scan images using the RDMF.
- The AW-BMVC method that precisely locates and isolates the impacted areas of the lung images is used in the segmentation procedure. By using SOSWT, the segmented images are subjected to feature extraction, where statistical and spectral features are extracted.
- Multi-Strategy RDCNN Classification Models with three alternative RDCNN models, each optimized with a unique optimization approach are used to classify the collected features: WHOA in conjunction with RDCNN-TriHorn-Net, AEALOA in RDCNN-

ResNeXt-50, DTOA in RDCNN-CoAtNet. When it comes to classifying lung CT scans the RDCNN-TriHorn-Net model, which has been optimised with WHOA, performs better than alternative approaches in terms of classification accuracy and detection precision.

Remaining paper is organised as: **Section2** explains the literature survey, **Section3** deliberates the materials and procedures utilized in this paper, **Section4** presents the outcomes with discussion, and **Section5** concludes this paper.

2. Literature survey

A number of researches were presented in the literature on automatic lung cancer detection from CT image, among these, some recent works are assessed here,

Shakeel et al., (2022) have presented enhanced Deep Neural Network (DNN) with ensemble classifier dependent automatic lung cancer finding from CT image. The multilayer brightness-preserving method effectively analyses every pixel, eradicates noise, and maximizes lung image quality. An improved deep neural network used network layers to partition the affected area of the noise-removed lung CT image and extract various features. It offers higher precision and higher mean absolute error.

(BR et al., 2024) have suggested the stacked neural nets for lung cancer categorization. The initial state of lung cancer was identified then examine the accurateness levels of several neural networks. Initially, image processing methods were used to extract lung sections. The segmentation procedure makes use of Stacked Neural Network (SNN). After the features extracted from the segmented images, various neural network approaches were applied for the classification process. It achieved high recall and low F-measure.

Chen et al., (2021) have suggested the LDNNET: towards robust categorization of lung nodule and cancer utilizing lung dense neural network. First it categorized lung nodules using LDNNET on the database and lung cancer using database; Second, evaluate lung CT images perform with respect to thick connections, pooling layers, and input pixel sizes; Thirdly, LDNNET used a dropout layer, dense connection, and data improvement to lessen overfitting. It has high sensitivity and less specificity.

Venkatesh et al., (2024) have introduced a hybrid method for lung cancer forecasting utilising patch processing with DL on CT images. An approach to lung cancer diagnosis was put out that uses deep learning techniques to detect the disease accurately and with less computing time. For these CT scans, image quality was enhanced through the application of median filtering and patches processing. After being pre-processed, images are sent into a Convolutional Neural Network (CNN) classifier after being segmented by a clustering segmentation procedure. It has higher precision and higher error rate.

Wankhade and Vigneshwari, (2023) have suggested a new hybrid deep learning approach for early lung cancer detection using neural networks. The deep neural networks were used to extract the features from the CT scan images. An advanced 3D-CNN was also used to increase diagnosis accuracy. Additionally, the suggested method makes it possible to distinguish between benign and malignant tumours. It provides high F1-score and less ROC.

Saha et al., (2024) have suggested hybrid transfer learning (TL) method for lung cancer identification utilising CT scan images. To identify lung cancer from lung CT scan pictures, a new transfer learning mode (VER-Net) that stacks three distinct TL models. Four classifications of lung cancer were used to train the algorithm to map CT scan images. To increase VER-Net's effectiveness, a number of techniques were used, including hyperparameter tuning, image preprocessing, and data augmentation. It offers higher F1-score and lower sensitivity.

Shashikala et al., (2024) have presented the Cross-spectral vision transformer with enhanced moth flame approach utilizing deep learning for lung nodule identification. First, compile databases from open-

source platforms. Preprocessing models such as filtering and contrast enhancement may be considered to eradicate unwanted noise from the input image. The image's necessary segmentation was completed utilising optimisation techniques and Automatic Lung cancer classification. It offers high specificity and low accuracy. Table 1 displays the literature survey table.

3. Proposed Methodology

In the proposed segment, the RDCNN-TriHorn-Net-WHOA-ALCD is described. Here, by starting, two Dataset's lung CT scan images are pre-processed using the RDMF to lower noise and enhance image quality. The AW-BMVC is used to segment the lung's impacted areas. SOSWT is used to extract spectral features. AEALOA, DTOA, and WHOA are three RDCNN-based models that are then given these features and optimised using various techniques. The RDCNN-TriHorn-Net model optimised with WHOA performs the best among them, with more accuracy in detecting lung cancer and classifying CT scan images. The description about the RDCNN-TriHorn-Net-WHOA-ALCD is given below. The block diagram of RDCNN-TriHorn-Net-WHOA-ALCD is illustrated in Fig. 1.

3.1. Image Acquisition

At first, the input lung CT scan imageries are taken via two datasets: (i) Chest CT-Scan Images -(<https://www.kaggle.com/datasets/addisisan/chest-ct-scan-images-dataset>, xxxx), (ii) Formatted and Augmented Chest CT-Scan images (<https://www.kaggle.com/datasets/benjaminmaizes/formatted-and-augmented-chest-ct-scan-images/data>, xxxx). On Chest CT-Scan Images database, these images provides detailed cross-sectional views of the chest, allowing for the recognition of abnormalities like tumours, nodules, and lesions. The data includes folders for three types of chest cancer. The data includes one folder for Adenocarcinoma, LCC, normal cells, SCC. The primary folder called data contains all of the step folders, comprising valid test and train. In Augmented Chest CT-Scan images dataset there are two directories in this dataset. One is actual 224×224 images from the dataset mentioned above. The other is a synthetic 224×224 image created with StyleGan2. Squamous cell lungs and normal cell lungs are depicted in both synthetic and genuine images. It contains images with training set 70 %, testing

set 20 % and validation set 10 %.

3.2. Pre-processing using Sub Aperture Keystone Transform Matched filtering

In this section, Sub Aperture Keystone Transform Matched Filtering (SAKTMF) (Zhan et al., 2023) is used for decreasing the noise and raises the lung image qualities. The SAKTMF technique successfully compensates for geometric distortions and focusing errors caused by non-idealities in the systems, hence improving the resolution of the images. The aperture is given by equation (1),

$$QR(k_t, k_n) = \sum_{l=1}^L QR_l(k_t, k_{n,l}) \quad (1)$$

where, QR represents the whole image, (k_t, k_n) denotes specificity of lung image structure, L indicates the sub blocks and l represents the sub aperture index. This step improves the lung tissue borders' clarity. Then, eliminating the noise is given in equation (2),

$$W\{\alpha\} = \sum_{l=1}^L \left| qR_l \left(\frac{2}{a} t(\alpha, ID_a), h(\alpha, ID_a) \right) \right| \quad (2)$$

here, α represents the searching elementary space vector, $t(\alpha, ID_a)$, and $h(\alpha, ID_a)$ represents the range and Doppler place according to sub aperture index l . Here, the input image is pre-processed by SAKTMF, which removes the noise and also maximize the lung image quality. These pre-processed data is fed into segmentation process.

3.3. Segmentation using automatically weighted binary Multi-View clustering

The segmentation using AW-BMVC (Houfar et al., 2023) is discussed for segmenting the affected regions of the lung images in this segment. A method for segmentation called AW-BMVC uses various data views or representations to enhance clustering quality. By combining various perspectives of the image and automatically allocating suitable weights to these perspectives according to their importance, AW-BMVC can assist in segmenting impacted areas in the context of medical image

Table 1
Literature Review.

Authors name	Objectives	Methods	Advantage	Limitation
Shakeel, et al., (2022)	To develop an automated lung cancer recognition system using enhanced DNNs and ensemble classifiers.	Enhance DNN, hybrid spiral optimization intelligent-generalized rough set method, multilevel brightness-preserving approach	It provides high precision.	It provides high mean absolute error
(BR et al., 2024)	To enhance classification accuracy in lung cancer detection by using stacked neural networks.	SNN, swarm intelligence-derived optimisation approaches, Sparrow Search Approach Grasshopper Optimisation Approach	It offers higher recall	It offers lower F-measure
Chen et al., (2021)	To develop a robust lung dense neural network for accurate classification of lung nodules and lung cancer.	median filtering, Deep dense neural network Laplacian filtering	It offers higher sensitivity	It offers lower specificity.
Venkateshet al., (2024)	To develop a hybrid approach for lung cancer prediction utilizing patches processing with DL techniques on CT images.	Median filtering, Particle Swarm optimization, CNN	It provides high processing time	It provides high Structure Similarity Index
Wankhade and Vigneshwari, (2023)	To develop a new hybrid deep learning model leveraging neural networks for the early and accurate identification of lung cancer.	3D-CNN, Residual Neural Network	It offers higher F1-score	It offers lower ROC
Saha et al., (2024)	To develop a HL learning for accurate lung cancer recognition utilizing CT scan images.	Random oversampling, VGG19, EfficientNetB0, and ResNet101	It offers higher F1-score	It offers lower sensitivity.
Shashikala, et al., (2024)	To develop a Cross-Spectral Vision Transformer for accurate lung nodule detection, optimized using an improved Moth Flame Algorithm to enhance deep learning	CSViT-IMFO	It offers higher specificity	It offers lower accuracy
RDCNN-TriHorn-Net-WHOA-ALCD (Proposed)	To develop an optimized Robust Deformed Convolutional Neural Network with TriHorn-Net for accurate and automated lung cancer detection from CT images.	RDMF, AW-BMVC, SOSWT, RDCNN, TriHorn-Net, ResNeXt-50, CoAtNet, AEALOA, DTOA, WHOA	It provides higher accuracy	Limited adaptability to rare subtypes

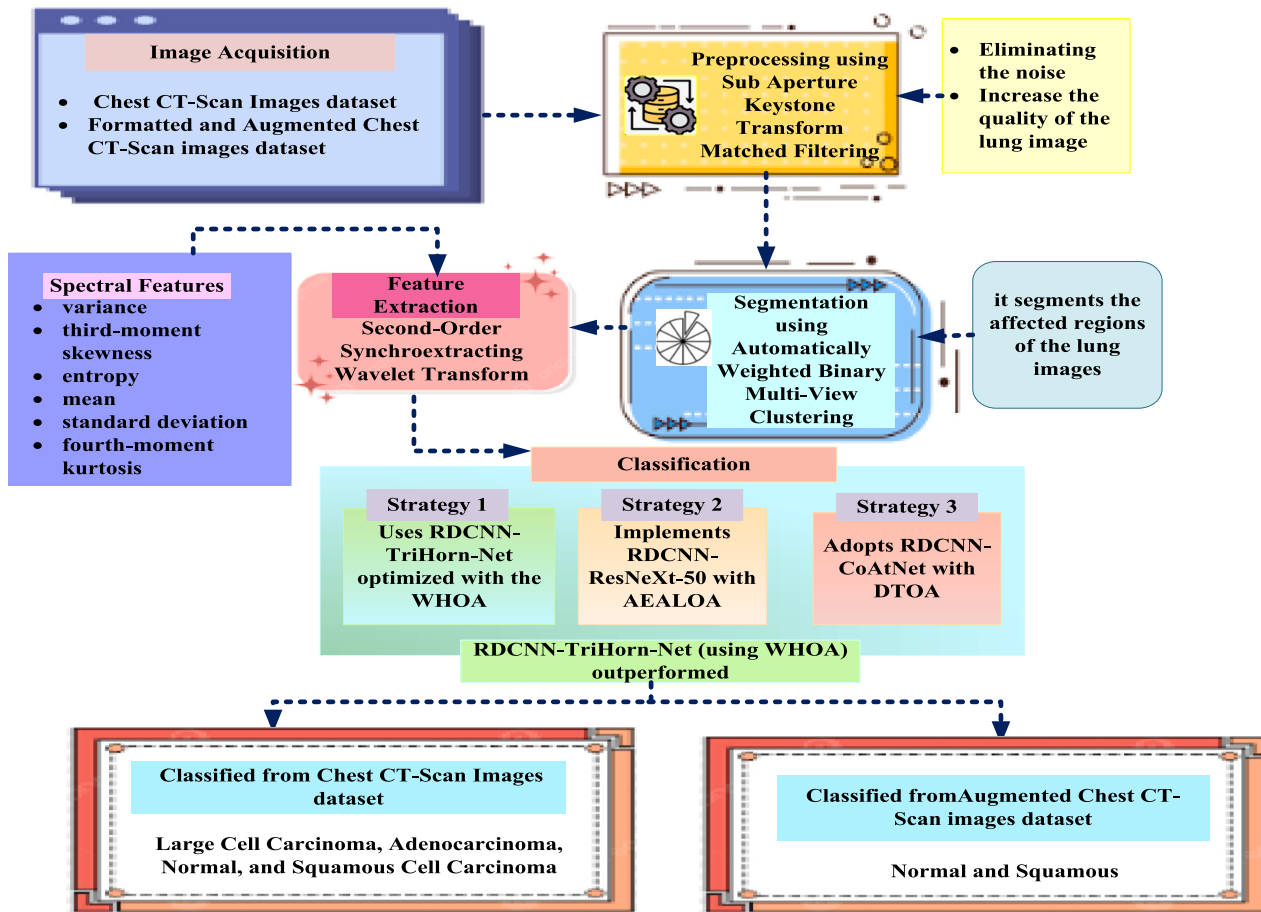


Fig. 1. Block Diagram of the Proposed RDCNN-TriHorn-Net-WHOA-ALCD Methodology.

segmentation, such as for the identification of lung cancer. AW-BMVC guarantees accurate segmentation, supports multiple views for increased precision, lowers noise, manages intricate lung structures, and enhances the identification of impacted lung regions. The algorithm performs clustering by assigning each pixel or region to one of two categories. This is done using a binary approach, often by solving an optimization problem that aims to find the best segmentation boundaries represented in equation (3),

$$\lambda(a_k^g) = \left[\exp\left(-\frac{\|a_k^g - a_1^g\|^2}{\phi^g}\right), \dots, \exp\left(-\frac{\|a_k^g - a_m^g\|^2}{\phi^g}\right) \right]^T \quad (3)$$

where $\{a_1^g, a_2^g, \dots, a_k^g\}$ indicates a collection of m particular anchors from the g^{th} view, ϕ^g denotes kernel width for g^{th} view, and $\lambda(a_k^g) \in H^g$ signifies m -size non-linear embedding for lung images from g^{th} view. The element-wise sign operator is $\text{sgn}(\cdot)$; and $\delta(a^g)$ represents matrix nonlinear illustration of every lung images in view g . Every view is automatically assigned a weight according to how much it adds to the segmentation process. This guarantees that the final clustering selection will be more influenced by the most pertinent attributes. Then, automatically weighted layer is expressed in equation (4),

$$y_k = r_k^g(\delta(a_k^g); P^g) = \text{sgn}(P^g \delta(a_k^g)) \quad (4)$$

where, the discrete clustering indications T and the binary clustering centroid Z are two matrices that are directly factorised from the learned discrete representation Y ; P^g represent the prioritized lung images. By efficiently merging data from many viewpoints, lowering noise, and improving the identification of pertinent features like tumors or nodules, weighted multi-view clustering raises the segmentation accuracy. Then

the binary clustered layer is represented in equation (5),

$$\min_{Z, t_k} \|y_k - Z t_k\|_L^2, \quad \text{s.t. } Z^T 1 = 0, Z \in \{-1, 1\}^{h \times z}, t_k \in \{0, 1\}^z, \sum_w t_{wk} = 1 \quad (5)$$

where the assignment vector for sample k is t_k , and the clustering centroids are Z . Based on pixel shape y_k and intensity t_{wk} , use weighted binary clustering to distinguish lung regions from non-lung areas. D is the dimensional phase of the images. This makes it possible to identify formations μ that resemble tumours. By using, AW-BMVC segments the affected regions of the lung images and supplied to the feature extraction process.

3.4. Feature extraction under second-order Synchro-extracting wavelet Transform

In this step, SOSEWT (Han et al., 2021) is discussed. Here, variance, entropy, mean, standard deviation, third-moment skewness, and fourth-moment kurtosis are among the spectral properties that are retrieved. By offering high-resolution spectrum information, the SOSWT improves feature extraction and makes it possible to precisely characterise lung disorders. It ensures a thorough representation of visual patterns by efficiently capturing important properties including variance, skewness, entropy, and kurtosis. It is labelled in equation (6),

$$\widehat{\omega}_a^{[2]}(T, x) = \widehat{\omega}_a(T, x) - \widehat{\omega}_a(T, x)(T - \widehat{T}_a(T, x)) \quad (6)$$

where, $\widehat{\omega}_a$ denotes the lung image functions; \widehat{T}_a represents the time duration T of every once iteration and $\widehat{\omega}_a$ indicates the growth in lung

image.

The extracted spectral features are described as follows,

Mean: The image's mean, which gives an indication of its overall brightness, is its average intensity. It is determined by equation (7),

$$\text{Mean}, \mu = \frac{1}{M} \sum_{a=1}^M D_a \quad (7)$$

where, D_a is the pixel intensity at position a , M represent the image dimension.

Standard Deviation: The standard deviation highlights contrast fluctuations by indicating the extent of variation or dispersion of pixel intensities around the mean. It is computed by equation (8),

$$\sigma = \sqrt{\frac{1}{M} \sum_{a=1}^M (D_a - \mu)^2} \quad (8)$$

Third-moment skewness: The asymmetry of the pixel intensity distribution is measured by skewness. It is calculated by equation (9),

$$sk = \left(\frac{1}{M * \sigma^3} * \sum_{a=1}^M (D_a - \mu)^3 \right)^{1/3} \quad (9)$$

Fourth-moment Kurtosis: The tailedness of the intensity distribution is measured by kurtosis. It is calculated by equation (10),

$$ku = \left(\frac{1}{M * \sigma^4} * \sum_{a=1}^M (D_a - \mu)^4 \right)^{1/4} \quad (10)$$

Entropy: Entropy quantifies an image's textural complexity or randomness. It is computed by equation (11),

$$\text{Entropy} = \sum_{a,b=0}^{m-1} -\ln(R_{ab})R_{ab} \quad (11)$$

Where, R_{ab} is the occurrence of intensity values at position a, b .

Variance: The dispersion of pixel intensities within an image is measured by variance. It is scaled by equation (12),

$$\text{Variance} = \sum_{a=0}^{m-1} \sum_{b=0}^{m-1} (a - \mu)^2 \cdot r(a, b) \quad (12)$$

where, $r(a, b)$ is the dispersion of intensity values at position a, b . Then the extracted features are given to classification.

3.5. Classification using Robust Deformed Denoising Convolutional neural Network

The classification using RDCNN is discussed here (Zhang et al., 2023). RDCNN is specifically intended to enhance image quality by efficiently eliminating noise. RDCNN is more resilient for complicated structures like tumours or lesions in lung CT scan images because it uses deformable convolutions, which allow it to adjust to changes in object forms or irregularities in the image. By adjusting the convolution kernels to the spatial properties of the lung images, these layers enable the model to concentrate on regions of interest (like tumours) irrespective of their location it is expressed by using equation (13).

$$S(z_p, z_q) = \sum_{h=1}^R R(z_p, z_q) N(z_p + \Delta p_j z_q + \Delta q) \quad (13)$$

where the coordinates of the centre point in a specific kernel S are represented by z_p and z_q . Its dimensions are set at 3×3 . Additionally, p_j stands for the offset of z_p in the horizontal and z_q in the vertical. These layers learn to distinguish edges, textures, and higher-level patterns, which are critical for spotting malignant growths. But for deformable convolution with kernel expressed in equation (14),

$$\left\{ (\Delta p_j, \Delta q_j) \right\} = \left\{ (-1 + D_{p1}, -1 + D_{q1}), \dots, (0 + D_{p5}, 0 + D_{q5}), \dots, (D_{p9}, 1 + D_{q9}) \right\} \quad (14)$$

where, D_{p1}, D_{q1} are the convolutional robust value. Additionally, contextual contact can enhance a deep network's learning capabilities.

To improve the accuracy, the RDCNN model for Automatic Lung Cancer recognition from Computed tomography image introduces three strategies as follows,

Strategy 1 – RDCNN-TriHorn-Net with WHOA: In this strategy, the RDCNN is used with the TriHorn-Net model optimized by the WHOA. This model is tested on different data ratios to evaluate its ability to detect lung cancer.

Strategy 2 – RDCNN-ResNeXt-50 with AEALOA: This strategy uses the ResNeXt-50 architecture combined with the AEALOA for further comparison.

Strategy 3 – RDCNN-CoAtNet with DTOA: The third strategy uses the CoAtNet model optimized by the DTOA. The three strategies are explained as follows:

3.5.1. Strategy 1: RDCNN-TriHorn-Net with WHOA

To increase the accuracy of feature extraction and classification, RDCNN incorporates the TriHorn-Net (Rezaei et al., 2023) architecture. Through the use of several levels of attention processes, the network is able to concentrate on important aspects of the CT images, like tumour regions. TriHorn-Net enables it to capture intricate information. This branch computes per-joint attention map $Attr_s^q \in \Psi^{Q \times h \times w}$ using encoder's output feature volume as input lung images. In order to do this, the attention map $Attr_s^q$ is first normalized using spatial softmax layer, which results in the matching heat map $K_q^{2D} = \sigma(Attr_s^q(r_p, s_q))$ is articulated in equation (15),

$$K_q^{2D}(a, b) = \frac{\exp(Attr_s^q(a, b))}{\sum_{r_p, s_p \in \kappa} \exp(Attr_s^q(r_p, s_q))} \quad (15)$$

where, the probability of the q^{th} joint happening at every pixel position is shown by the heat map K_q^{2D} . The attention map $Attr_s^q(r_p, s_q)$ spatial domain is represented by σ . Using an integration process akin to, the 2D position of the q^{th} joint is determined.

3.5.1.1. Optimization under Wader Hunt optimization Algorithm. The weights parameter z_p and s_p of RDCNN-TriHorn-Net is enhanced with the WHOA (Vasantrao and Gupta, 2023). The weight parameter z_p is optimized to increase the accuracy, as well as s_p is optimized to decrease the mean absolute error. Benefits of the WHOA include robustness in complex model optimisation, quick convergence, and effective global search capabilities. It is especially useful for fine-tuning RDCNN for lung cancer diagnosis since it adjusts to changing conditions, improving accuracy and precision in parameter adjustment. The stepwise process of the WHO algorithm is provided below.

Stepwise process of WHO Algorithm

The stepwise procedure is determined to acquire best value of RDCNN-TriHorn-Net depends on WHO Algorithm. Initially, WHOA creates the equal distributing populace to enhance the parameter of RDCNN-TriHorn-Net.

Step 1: Initialization

The population of WHOA contains Wader Hunt, which Search for better solutions by changing their populations in the search space. Every Wader Hunt is a WHOA population member. It is given in equation (16),

$$X = \begin{bmatrix} x_{11} & x_{12} & x_{13} & \dots & x_{1e} \\ x_{21} & x_{22} & x_{23} & \dots & x_{2e} \\ \dots & \dots & \dots & \dots & \dots \\ x_{n1} & x_{n2} & x_{n3} & \dots & x_{ne} \end{bmatrix} \quad (16)$$

Let the population of Wader Hunt Optimization is initialized as x and its respective positioning as x_n . Wader Hunt's initial position at the search location is randomly determined at the beginning of the WHOA process.

Step 2: Random generation

Create the input parameters randomwise. The better fitness selection is depending on the explicit hyper parameter situation.

Step 3: Estimation of Fitness Function

Fitness function is assessed using optimization variable value to maximize weight variable z_p and s_p of RDCNN-TriHorn-Net is formulated in equation (17),

$$\text{Fitness Function} = \text{optimizing } [z_p \text{ and } s_p] \quad (17)$$

Step 4: Attacking Phase for optimizing z_p and s_p

The group members who live and targeted by the scavengers when they look for prey and travel away from each other to attack it. Therefore, using this search strategy improves the behaviour of global searches is given in equation (18),

$$N = \frac{1}{R} s_p \sum_{j=1}^R z_p (B_j - \vec{B}_j)^2 \quad (18)$$

where, N signifies the total sample, \vec{B}_j indicates the targeted output, B_j referred as the targeted output, R signifies the position of the other scavengers, N implies feasibility solution and j indicates the prey's location.

Step 6: Termination

The weight parameter z_p and s_p from RDCNN-TriHorn-Net are optimized using WHOA, will continue till the position information is obtained $X = X + 1$ is met. Since WHOA is supposed to be the most adept at fine-tuning the parameters, RDCNN-TriHorn-Net-WHOA is anticipated to deliver the optimal performance in terms of accuracy and precision.

3.5.2. Strategy 2: RDCNN-ResNeXt-50 with AEALOA

By utilising ResNeXt-50 (Tripathi et al., 2022) architecture for effective learning and RDCNN's capacity to extract intricate, spatially variable features from CT scan images, this model performs exceptionally well in the classification of lung cancer. Neurons in neural networks perform inner product that is similar to combining the AT lung images and it is represented as in equation (19),

$$AT = \sum_{u=1}^H m_u a_u \quad (19)$$

here H stands for the input vector of neuron's H channel, $x = [x_1, x_2, \dots]$, filter weight for u^{th} channel is indicated by m_u . The group size of variations to be amassed referred to as network's cardinality (H) can include any lung images.

3.5.2.1. Optimization using Adaptive Elite ant lion Optimizer. AEALO (Panneer and Jaganathan, 2024) ensures that the RDCNN-ResNeXt-50 wt parameters $\Delta q_j \& \kappa_u$ are optimized for superior performance, resulting in improved accuracy. AEALO is applied to enhance the weight parameters of RDCNN-ResNeXt-50, with one parameter being optimized to Δq_j higher recall and κ_u to lower logarithm loss. One of its key advantages is its ability to achieve global optimization, preventing the RDCNN-ResNeXt-50 from getting trapped in local minima during training. The following steps cover the six primary stages of the AEALO algorithm principle.

Stepwise Procedure for AEALOA.

Here, step-by-step procedure is outlined to optimize the RDCNN-ResNeXt-50 using the AEALO. Initially, AEALO allocates the population equally to improve the parameters of the RDCNN-ResNeXt-50. The most promising solutions are identified through the AEALO process.

Step 1: Initialization

The model is expressed in the initialization weight parameter as a predictor of water quality, and this is utilized to compute the modulation detection in the RDCNN-ResNeXt-50 wt parameters is calculated by equation (20),

$$P = \begin{bmatrix} P_{1,1} & P_{1,2} & \dots & P_{1,b} \\ P_{2,1} & P_{2,2} & \dots & P_{2,d} \\ \vdots & \vdots & \vdots & \vdots \\ P_{n,1} & P_{n,2} & \dots & P_{n,b} \end{bmatrix} \quad (20)$$

here P specifies parameter weight calculation for ant, $P_{n,b}$ indicates amount of parameter weight calculation for lion.

Step 2: Random generation

The weight parameter $\Delta q_j \& \kappa_u$ creates randomly through AEALO after that initialization process.

Step 3: Fitness Function

It generates random solution through initialization. AEALO approach is used to evaluate the fitness of each position vector that corresponds to each piece of data. Fitness function is determined by equation (21),

$$\text{Fitness Function} = \text{optimizing } [\Delta q_j \text{ and } \kappa_u] \quad (21)$$

Step 4: Hunting phase for Optimizing Δq_j and κ_u

To select an ant lion, use the roulette wheel selection process to update each ant's position. Each optimization vector is calculated by equation (22),

$$U_a^{h+1} = \omega U_a^h + \kappa_u \Delta q_j e_1 g_1 (qbest^h - a_a^h) + e_2 g_2 (qbest^h - a_a^h) \quad (22)$$

where U_a^{h+1} denotes the iteration velocity of particle, ωU_a^h epitomizes present count of iterations, e_1, e_2 symbolizes acceleration coefficients, g_1, g_2 implicates random numbers of the interval, $qbest^h$ implies best position amongst all iterations, a_a^h denotes non-negative inertial weight factor.

Step 5: Termination

At last, the factor $\Delta q_j \& \kappa_u$ is optimized by AEALO; otherwise repeat step 3 till it reaches halting criteria $P = P + 1$. Although better results are anticipated from RDCNN-ResNeXt-50-AEALOA, ResNeXt-50 might not be as effective as TriHorn-Net in this work.

3.5.3. Strategy 3: RDCNN-CoAtNet with DTOA

To identify and categorise lung cancer from CT scan pictures, RDCNN-CoAtNet, a sophisticated hybrid model, combines RDCNN with CoAtNet (Tripathi et al., 2022). This architecture efficiently detects tumours or aberrant tissue in medical images like as CT scans by utilising the advantages of both transformer and convolutional models to capture both local and global data. CoAtNet offers state-of-the-art performance with changing data while utilizing the same resource, volumes. Depth wise convolution, where each channel undergoes independent convolution is labelled in equation (23),

$$C_p = \sum_{q \in \mathcal{N}(p)} m_{p-q} \otimes D_q \quad (23)$$

where $C_p, D_q \in K^S$ denotes input, output at place p ; $\mathcal{N}(p)$ represents local region of p , like grid centred on p in lung image position. The layers enable the model to discover subtle patterns of cancer spread by capturing global relationships within lung CT scan images higher accuracy is obtained by employing RDCNN-CoAtNet, after which it is sent to DTOA.

3.5.3.1. Optimization using Dipper Throated optimization Algorithm (DTOA). The weight parameters R_{DD} , and d_q of the proposed RDCNN-CoAtNet are optimized through the Dipper Throated Optimization Algorithm (Abdelhamid et al., 2023). The weight parameter R_{DD} is optimized to increase the F1-score, and d_q is optimized to decrease the error rate. By adaptively balancing exploration and exploitation, the DTOA improves performance when used to optimise RDCNN. By fine-tuning the RDCNN's hyperparameters, the following steps cover the five main stages that comprise up the DTO algorithm principle.

Stepwise procedure of DTOA.

Here, the stepwise process is defined using DTOA to obtain the optimal value of RDCNN-CoAtNet. To optimise the RDCNN-CoAtNet settings, DTOA first creates an evenly dispersed population. The stepwise procedure is delineated below.

Step 1: Initialization

Initialize the weight parameters, which is illustrated in the form of enabled recognition for RDCNN-CoAtNetApplication. This is employed to compute the lung cancer detection using the weight factors in equation (24),

$$D = \begin{bmatrix} d_{1,1} & d_{1,2} & \dots & d_{1,z} \\ d_{2,1} & d_{2,2} & \dots & d_{2,z} \\ \vdots & \vdots & \vdots & \vdots \\ d_{N,1} & d_{N,2} & \dots & d_{N,z} \end{bmatrix} \quad (24)$$

here d signifies dipper population, $d_{N,z}$ represents the count of birds.

Step 2: Random generation

After initialization, the weight parameter is randomwise generated through DTO.

Step 3: Fitness Function

The fitness function is produced arbitrarily from the initialized evaluations. The parameter optimization improve the weight parameter R_{DD}, d_q by equation (25),

$$\text{Fitness function} = \text{optimizing}[R_{DD}, d_q] \quad (25)$$

Step 4: Exploration for optimizing R_{DD}, d_q

To explore new locations, DTOA imitates the bird's behaviour of diving into deeper areas during the exploration phase. In uncharted areas of the solution space, this aids the algorithm's search for superior solutions is exhibited in equation (26),

$$y = q_{par}(c) - R_{DD}, d_q d_1.d_2.q_{par}(c) - q(d)R_{DD} \quad (26)$$

here y represents adjustment of position, $q_{par}(c)$ represents search space boundaries d_1, d_2 is the dimensionalities of the birds, $q(d)$ refers quality of updating position.

Step 5: Termination

This stage involves applying DTOA to improve the weight parameter values, R_{DD} , and d_q , of RDCNN-CoAtNet. The 3rd step is repetitive until the halting requirement, $D = D + 1$, is satisfied. Here, RDCNN-CoAtNet-DTOA gives due to the relative complexity of the architecture, it is anticipated that this model will perform rather well, although it will probably be surpassed by the other two.

Finally, Strategy 1 (RDCNN-TriHorn-Net with WHOA) works better than the other methods and achieves a higher detection accuracy for lung cancer. Its effectiveness was confirmed by reporting reduced logarithmic loss and higher Dice similarity coefficients when compared to Strategy 2 (RDCNN-ResNeXt-50 with AEALOA) and Strategy 3 (RDCNN-CoAtNet with DTOA).

3.6. Computational complexity

Time complexity during fitness estimation with maximum iterations $Maxgen$, objectives f , populace size $Popsize$ as $O(Maxgen \times f \times Popsize)$. Initializing the population takes $O(Popsize \times f)$ of time. The WHOA needs $O(f \times (s + Popsize))$ time to archive update in non-dominate so-

lutions, here σ indicates optimum search agents. Therefore, the total time complexity of proposed system signifies $O(Maxgen \times f \times (Popsize + s) \times L)$, space complexity in the period of creation of population in storage necessitates $O(Popsize \times f)$ time. The archive updation and fitness computation process is repeated until attains maximal iterations. The WHOA's time complexity along N input is $O(N^3)$. Hence, the total time complexity of the Reviewer Reliability with Automatic Lung Cancer Diagnosis from CT image with the help of Optimized Robust Deformed Convolutional Neural Network with TriHorn-Net represents $O(N^3 \times Maxgen \times f \times Popsize)$ respectively.

4. Result and discussion

The proposed fine-tuned RDCNN-TriHorn-Net with WHOA is implemented in Google Colab Pro framework which allows faster training and assessment of the method, which is useful to test the proposed approach. The experimental setup used in this work is as follows: This research done in Windows operating system using Python 3.8 and Pytorch 1.8.2, Nvidia RTX3060Ti GPU, AMD 6900HX CPU, the Keras library and Tensor Flow as a backend to train the method. The experiments are carried out in Tesla T4 GPU on Google Colab Pro, which has 25 GB of RAM and examined utilizing mentioned performance measures. The acquired outcomes of the proposed RDCNN-TriHorn-Net-WHOA-ALCD technique are evaluated with existing ALCD-IDNN-CTI (Shakeel et al., 2022), CLC-SNN-CTI (BR et al., 2024) and RC-DNN-LNC (Chen et al., 2021) methods respectively.

Table 2 depicts hyper parameters of the RDCNN-TriHorn-Net-WHOA-ALCD method. By deactivating neurons randomly while training, a dropout rate of 0.2 aids in preventing overfitting. By adding non-linearity, ReLU activation helps the model discover intricate patterns. The accuracy of gradient estimation and computing performance are balanced at a batch size of 32. Training may be accelerated by the comparatively large steps made possible by the learning rate of 5. A population size of 100 for the optimization method strikes a balance between exploration and exploitation, and a maximum of 300 iterations gives the process enough time to converge. Combining solutions promotes exploration when the crossover rate is 0.6. Lastly, a convergence threshold of 0.08 stops the optimization process when the objective function improvement is negligible, avoiding needless computation. AEALOA uses ant lion behavior to optimize hyperparameters such as adaptive weight factor of 0.8, elite selection probability of 0.6 and population size of 40. By utilizing the DTOA optimizes hyperparameters such as population size of 45, maximum iterations of 180, exploration-to-exploitation ratio of 0.5, and mutation probability of 0.2. These hyper parameter selections were probably made by combining experimentation with best practices in evolutionary and deep learning. Fig. 2 shows the output of the proposed RDCNN-TriHorn-Net-WHOA-ALCD Method.

4.1. Performance measures

The efficacy of the RDCNN-TriHorn-Net-WHOA-ALCD method is estimated under the mentioned measures. The following matrixes are

Table 2

Hyper parameters of the proposed approach.

Hyper parameters	Values	Hyper parameters	Values
Dropout rate	0.2	AEALOA	
Dense layer Activation	ReLU	Population size	40
Batch size	32	Maximum iterations	150
Learning rate	5	Elite selection probability	0.6
WHOA		DTOA	
Population size	100	Population size	45
Maximum iterations	300	Maximum iterations	180
Crossover Rate	0.6	Exploration-to-exploitation ratio	0.5
Convergence threshold	0.08	Mutation probability	0.2

Input Image	Preprocessed Image	Segmented Image	Classification
			Adenocarcinoma
			Large Cell Carcinoma
			Normal
			Squamous Cell Carcinoma

Fig. 2. Output of the proposed RDCNN-TriHorn-Net-WHOA-ALCD method using Chest CT-Scan images dataset.

required to compute the performance metrics.

- True positive (TP): samples where the method properly predicts a positive class
- True Negative (TN): samples where the method properly predicts a negative class.
- False Positive (FP): samples where the method wrongly predicts a sample as belonging to a positive class.
- False Negative (FN): samples where the method wrongly predicts a sample as negative belonging to a positive class

4.1.1. Accuracy

It is determined by dividing a number of correctly predicted instances by the total number of cases using equation (27),

$$\text{Accuracy} = \frac{\text{TP} + \text{TN}}{\text{TP} + \text{TN} + \text{FP} + \text{FN}} \quad (27)$$

4.1.2. Recall

Sensitivity is defined as the percentage of TPs to entire FPs and true positives. It is computed through equation (28),

$$\text{Recall} = \frac{\text{TP}}{\text{TP} + \text{FN}} \quad (28)$$

4.1.3. F1-score

F-score challenges methods with greater specificity and rewards methods with higher sensitivity. This is computed using equation (29),

$$\text{F1 Score} = 2 * \frac{\text{Precision} * \text{Recall}}{\text{Precision} + \text{Recall}} \quad (29)$$

4.1.4. Mean absolute error (MAE)

This is the average absolute distinguishes among expected and actual values. It is computed by equation (30),

$$MSE = \sum_{a=1}^n |b_a - \hat{b}_a| \quad (30)$$

Where, b_a denotes actual value, \hat{b}_a indicates predicted value, n implicates number of data points.

4.1.5. Dice similarity Index

By comparing the intersection size of two sets (or regions in images) to their total size, the Dice Similarity Index calculates how similar the two sets are. It is calculated by using equation (31),

$$DSI = \frac{2 \times |X \cap Y|}{|X| + |Y|} \quad (31)$$

where, X implicates set of predicted positive pixels and Y implicates set of actual positive pixels.

4.1.6. Logarithmic loss

The disparity among the actual distribution (the true labels) and the projected probability distribution is assessed using equation (32),

$$\log loss = -\frac{1}{M} \sum_{a=1}^M [b_i \log(s_a) + (1 - b_a) \log(1 - s_a)] \quad (32)$$

where, M implies number of samples, b_i implies true label of the i^{th} sample, s_a refers predicted probability of the sample.

4.1.7. Error rate

It is the proportion of wrongly categorized to all instances counted and determined by equation (33),

$$\text{Error Rate} = 100 - \text{Accuracy} \quad (33)$$

4.2. Performance analysis

4.2.1. Analysis on Chest CT-Scan images dataset

Figs. 3 to 5 and Tables 3, 4 shows simulation outcomes of RDCNN-TriHorn-Net-WHOA-ALCD technique under Chest CT-Scan Images dataset. Then, the performance of the RDCNN-TriHorn-Net-WHOA-ALCD technique are compared with existing ALCD-IDNN-CTI, CLC-SNN-CTI and RC-DNN-LNC models.

Fig. 3 depicts performance analysis of accuracy. The optimized convolutional network of the RDCNN-TriHorn-Net-WHOA-ALCD model improves feature extraction from CT images, resulting in a high accuracy in autonomous lung cancer detection. TriHorn-Net enhances accuracy by identifying minor image patterns and optimizing performance. The proposed RDCNN-TriHorn-Net-WHOA-ALCD method attains 18.34 %, 16.23 %, 19.56 % better accuracy for Adenocarcinoma; 16.07 %, 17.56 % and 15.44 % better accuracy for large cell carcinoma; 12.33 %, 15.23 % and 17.35 % better accuracy for normal; 16.26 %, 19.34 % and 21 % better accuracy for Squamous cell carcinoma compared with existing ALCD-IDNN-CTI, CLC-SNN-CTI and RC-DNN-LNC models.

Fig. 4 depicts performance of dice similarity coefficient. The Robust Deformed CNN with TriHorn-Net, optimized using Wader Hunt Optimization demonstrates superior performance in automatic lung cancer detection by effectively aligning features, handling irregular tumor shapes, and enhancing segmentation accuracy, leading to a high Dice Similarity Index. The RDCNN-TriHorn-Net-WHOA-ALCD method attains 13.67 %, 27.55 % and 14.67 higher Dice Similarity coefficient for Adenocarcinoma; 23 %, 13.44 % and 14.78 % higher Dice Similarity coefficient for large cell carcinoma; 22.56 %, 26.38 % and 12.33 % higher Dice Similarity coefficient for normal; 13.23 %, 16.56 % and 17.34 % higher Dice Similarity coefficient for squamous cell carcinoma than the existing ALCD-IDNN-CTI, CLC-SNN-CTI and RC-DNN-LNC models.

Fig. 5 portrays logarithmic loss analysis. As the RDCNN-TriHorn-Net-WHOA-ALCD model can minimize the error between projected probabilities and actual outcomes, logarithmic loss is minimal in Automatic Lung Cancer Detection. Accuracy is improved through optimization with RDCNN and TriHorn-Net, which leads to accurate cancer identification and decreased log loss. The RDCNN-TriHorn-Net-WHOA-ALCD method attains 22.23 %, 24.11 % and 25.56 % lower Logarithmic loss for Adenocarcinoma; 17.34 %, 19.54 % and 20.56 % lower Logarithmic loss for large cell carcinoma; 21.34 %, 24.15 % and 26.24 % lower Logarithmic loss for normal; 22.34 %, 26.45 % and 22.56 % lower Logarithmic loss for Squamous cell carcinoma over the existing ALCD-IDNN-CTI, CLC-SNN-CTI and RC-DNN-LNC models.

Table 3 depicts MAE and recall analysis. The Mean Absolute Error (MAE) is low for RDCNN-TriHorn-Net-WHOA-ALCD because the model precisely aligns features, tolerates irregular tumor shapes, and

effectively segments tumors. The optimization ensures accurate prediction of boundaries, minimizing discrepancies between predicted and actual values, resulting in reduced errors. The RDCNN-TriHorn-Net-WHOA-ALCD method attains 18.56 %, 22.02 % and 17 % lower MAE for Adenocarcinoma; 17.22 %, 27.34 %, and 14.33 %; lower MAE for large cell carcinoma; 14.22 %, 16.37 % and 17.45 % lower MAE for normal; 13.56 %, 15.67 % and 17.55 % lower MAE for squamous cell carcinoma than the existing ALCD-IDNN-CTI, CLC-SNN-CTI and RC-DNN-LNC models. The ability of the RDCNN-TriHorn-Net-WHOA-ALCD model to correctly identify real positive instances of lung cancer is probably the reason for the high recall in Automatic Lung Cancer Detection from CT images. The RDCNN's sensitivity to identify small or subtle malignant patches is improved through TriHorn-Net optimization, which also improves recall. The RDCNN-TriHorn-Net-WHOA-ALCD method attains 16.55 %, 24.12 % and 27.22 % higher recall for Adenocarcinoma; 13.99 %, 12.09 % and 11.45 % higher recall for large cell carcinoma; 15.66 %, 16.45 % and 17.88 % higher recall for normal; 22.45 %, 24.33 % and 26.38 % higher recall for squamous cell carcinoma compared to the existing ALCD-IDNN-CTI, CLC-SNN-CTI and RC-DNN-LNC models.

Table 4 depicts F1-score and error rate analysis. The RDCNN-TriHorn-Net-WHOA-ALCD model's high F1-score in Automatic Lung Cancer Detection from CT Image propose a good trade-off between recall and precision. This implies that the algorithm is successfully detecting lung cancer with accuracy and dependability by minimizing false positives and negatives and identifying real positives. The RDCNN-TriHorn-Net-WHOA-ALCD method attains 18.36 %, 20.45 % and 21.67 % higher F1-score for Adenocarcinoma; 25.67 %, 26.45 % and 27.34 % higher F1-score for large cell carcinoma; 22.34 %, 25.38 % and 27.45 % higher F1-score for normal; 12.33 %, 16.39 %, 22.46 % higher recall for squamous cell carcinoma over the existing ALCD-IDNN-CTI, CLC-SNN-CTI and RC-DNN-LNC models. The percentage of inaccurate predictions provided by the proposed model is reflected in the error rate for automatic lung cancer detection utilizing the RDCNN-TriHorn-Net-WHOA-ALCD approach. By using TriHorn-Net and an optimized RDCNN architecture, lung cancer can be more accurately identified from CT images with a lower error rate, improving detection precision. The RDCNN-TriHorn-Net-WHOA-ALCD method attains 12.49 %, 16.59 %, 18.28 % less error rate for Adenocarcinoma; 15.59 %, 17.38 %, 18.78 %; less error rate for large cell carcinoma; 11.28 %, 14.47 %, 18.11 % less error rate for normal; 17.48 %, 18.55 % and 19.76 % lower error rate for squamous cell carcinoma compared with the existing ALCD-IDNN-CTI, CLC-SNN-CTI and RC-DNN-LNC models.

4.2.2. Performance analysis on Formatted and Augmented Chest CT-Scan images dataset

Table 5 shows simulation outcomes of RDCNN-TriHorn-Net-WHOA-

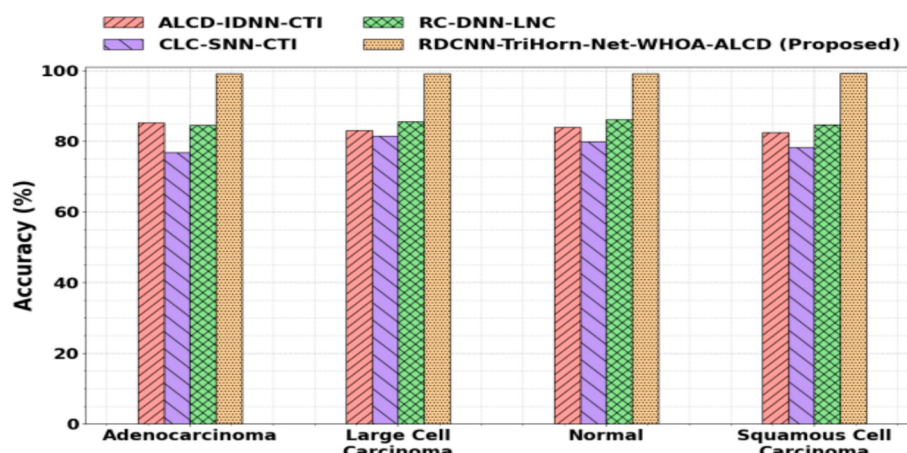


Fig. 3. Performance analysis of accuracy.

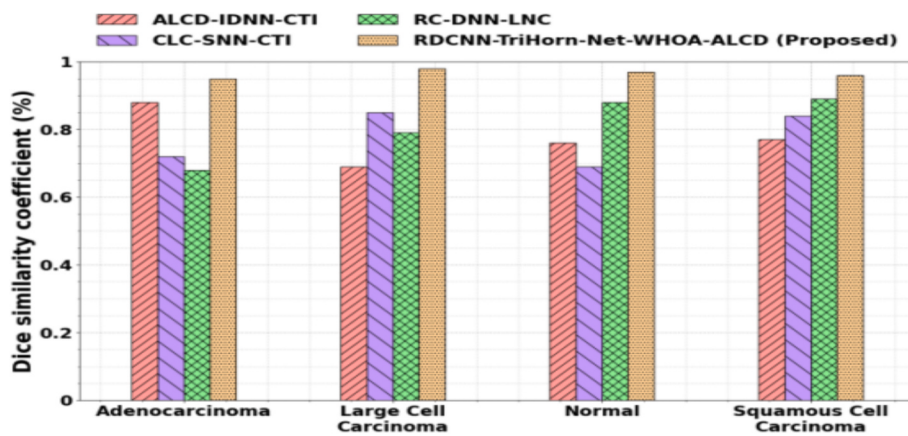


Fig. 4. Performance of dice similarity coefficient.

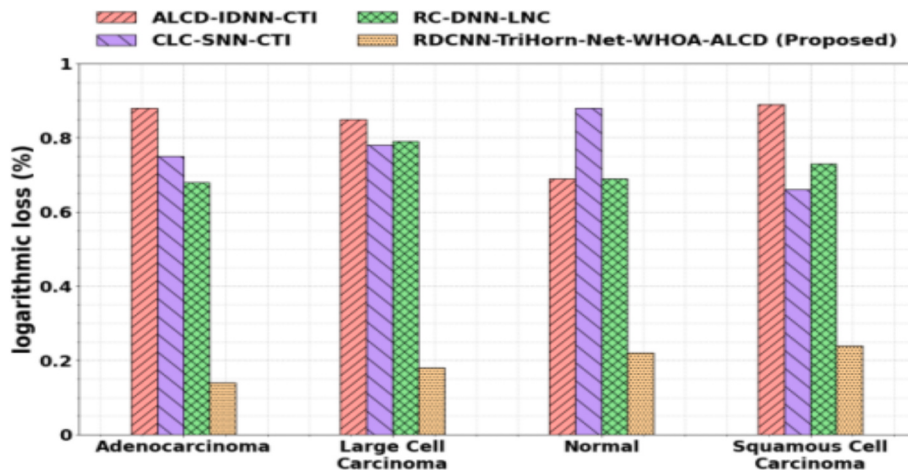


Fig. 5. Performance of logarithmic loss.

Table 3
Performance analysis of MAE and recall.

Methods	MAE (%)				Recall (%)			
	Adeno carcinoma	Large Cell Carcinoma	normal	Squamous Cell Carcinoma	Adeno carcinoma	Large Cell Carcinoma	normal	Squamous Cell Carcinoma
ALCD-IDNN-CTI (Shakeel et al., 2022)	14.8	16.9	16	17.5	70.58	83.56	91.62	90.58
CLC-SNN-CTI (BR et al., 2024)	23.2	18.6	20.1	21.8	86.53	74.88	80.36	88.78
RC-DNN-LNC (Chen et al., 2021)	15.5	14.5	13.9	15.3	79.65	78.50	94.60	94.50
RDCNN-TriHorn-Net-WHOA-ALCD (Proposed)	0.88	0.86	0.84	0.82	98.5	98.2	98.8	98.1

Table 4
Performance of F1-score and error rate.

Methods	F1-score (%)				Error rate (%)			
	Adeno carcinoma	Large Cell Carcinoma	normal	Squamous Cell Carcinoma	Adeno carcinoma	Large Cell Carcinoma	normal	Squamous Cell Carcinoma
ALCD-IDNN-CTI (Shakeel et al., 2022)	71.58	83.34	78.22	81.58	14.8	16.9	17.516	16
CLC-SNN-CTI (BR et al., 2024)	78.53	74.27	88.34	78.46	23.2	18.6	21.8	20.1
RC-DNN-LNC (Chen et al., 2021)	83.65	82.50	80.34	86.50	15.5	14.5	15.3	13.9
RDCNN-TriHorn-Net-WHOA-ALCD (Proposed)	98.01	98.07	98.11	98.09	0.88	0.86	0.82	0.84

Table 5

Comparative analysis on Formatted and Augmented Chest CT-Scan images dataset.

Methods	Accuracy (%)	Precision (%)	Dice similarity coefficient (%)	Logarithmic loss (%)
ALCD-IDNN-CTI (Shakeel et al., 2022)	82.5	82.22	0.88	0.77
CLC-SNN-CTI (BR et al., 2024)	78.2	86.34	0.72	0.84
RC-DNN-LNC (Chen et al., 2021)	84.70	88.21	0.68	0.89
RDCNN-TriHorn-Net-WHOA-ALCD (Proposed)	99.58	98.56	0.96	0.24

ALCD technique using Formatted and Augmented Chest CT-Scan images dataset. Then, the proposed RDCNN-TriHorn-Net-WHOA-ALCD techniques are compared with existing ALCD-IDNN-CTI, CLC-SNN-CTI and RC-DNN-LNC models.

Table 5 depicts the comparative analysis on formatted and augmented chest CT-scan images dataset. The high accuracy RDCNN-TriHom-Net-WHOA-ALCD is due to its robust feature alignment, ability to handle irregular tumor shapes, and improved AW-BMVC. The RDCNN-TriHom-Net-WHOA-ALCD excellent precision in automatic lung cancer diagnosis is ascribed to the model's precise tumor region classification, which lowers false positives. Its enhanced segmentation, tolerance for unusual tumor shapes, and strong feature alignment guarantee accurate lung cancer diagnosis. The high Dice similarity coefficient indicates excellent overlap among the predicted and ground truth lung cancer regions, demonstrating that the Robust Deformed CNN with TriHorn-Net and Wader Hunt optimization accurately detects lung cancer. Logarithmic loss is low in this proposed model because it effectively minimizes the difference between predicted and true probabilities, enhancing classification accuracy, especially when using robust, optimized CNN architectures for lung cancer detection. The proposed RDCNN-TriHorn-Net-WHOA-ALCD method achieved superior lung cancer classification with 99.58 % accuracy, 98.56 % precision, 0.96 % Dice similarity coefficient, and a low 0.24 % logarithmic loss, outperforming existing methods.

Fig. 6 shows computational complexity analysis. The curves show that as input size increases, CPU operation grows for all methods. However, the proposed RDCNN-TriHorn-Net-WHOA-ALCD

demonstrates the flattest curve, indicating lower computational complexity and suggesting it scales more efficiently with larger input sizes compared to ALCD-IDNN-CTI, CLC-SNN-CTI, and RC-DNN-LNC respectively.

Table 6 shows the comparison of Three Strategies of RDCNN model. With the best accuracy (99.35 %), recall (98.45 %), and F1-score (96.67 %), Strategy 1 (RDCNN-TriHorn-Net with WHOA) proved to be the efficient method for identifying lung cancer while striking a balance between sensitivity and precision. RDCNN-ResNeXt-50 with AEALOA is the second strategy performed admirably as well, with an F1-score of 94.73 %, recall of 97.56 %, and accuracy of 99.19 %, suggesting successful identification but marginally worse performance than Strategy 1. Despite its effectiveness, strategy 3 (RDCNN-CoAtNet with DTOA) had the lowest performance, F1-score 93.38 %, accuracy 98.55 %, and recall 96.21 %. The findings indicate that, out of all the techniques examined, RDCNN-TriHorn-Net with WHOA is the most successful model for perceiving lung cancer because to its high accuracy and balanced detection metrics.

Table 7 depicts the cost analysis of the proposed method. The computational and implementation expenses of ALCD-IDNN-CTI are \$700 and \$2400, respectively. The cost of CLC-SNN-CTI are \$2200 and \$650. \$500 and \$2500 are incurred by RC-DNN-LNC. The suggested RDCNN-TriHorn-Net-WHOA-ALCD approach is more affordable, and requiring only \$400 for compute and \$1500 for implementation.

Table 8 shows training and test accuracies, along with the running times for various models. The proposed RDCNN-TriHorn-Net-WHOA-ALCD model demonstrates superior performance with a training accuracy of 99.1 % and a testing accuracy of 98.7 %, surpassing other models like ALCD-IDNN-CTI with 95.6 % train, 92.3 % test, CLC-SNN-CTI with 93.8 % train, 89.4 % test, and RC-DNN-LNC with 94.2 % train, 90.1 % test. Furthermore, the proposed model achieves these high accuracies with significantly faster training and testing times (2 h training, 5 min testing) compared to the others.

Table 9 presents the statistical significance testing using ANOVA for lung cancer classification. The variability between groups, with three

Table 6
Comparison of Three Strategies of RDCNN model.

Strategy	Methods	Accuracy (%)	Recall (%)	F1-score (%)
Strategy 1	RDCNN-TriHorn-Net with WHOA	99.35	98.45	96.67
Strategy 2	RDCNN-ResNeXt-50 with AEALOA	99.19	97.56	94.73
Strategy 3	RDCNN-CoAtNet with DTOA	98.55	96.21	93.38

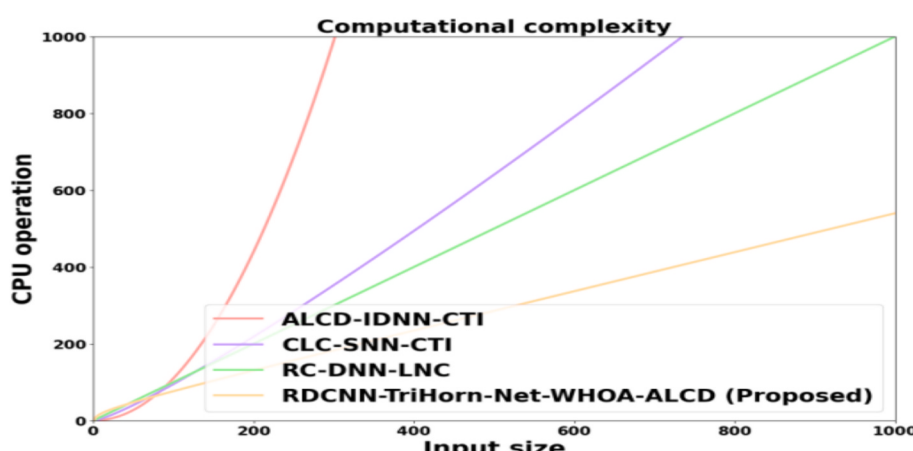


Fig. 6. Performance of computational complexity.

Table 7
Cost analysis of the proposed Method.

Methods	Computational Cost (\$)	Implementation Cost (\$)
ALCD-IDNN-CTI (Shakeel et al., 2022)	700	2400
CLC-SNN-CTI (BR et al., 2024)	650	2200
RC-DNN-LNC (Chen et al., 2021)	500	2500
RDCNN-TriHorn-Net-WHOA-ALCD (proposed)	400	1500

Table 8
Training and Test accuracies, along with the running times for various models.

Model	Train Accuracy (%)	Test Accuracy (%)	Running Time (Training)	Running Time (Testing)
ALCD-IDNN-CTI (Shakeel et al., 2022)	95.6	92.3	5 h	6 min
CLC-SNN-CTI (BR et al., 2024)	93.8	89.4	7 h	8 min
RC-DNN-LNC (Chen et al., 2021)	94.2	90.1	4 h	6 min
RDCNN-TriHorn-Net-WHOA-ALCD (proposed)	99.1	98.7	2 h	5 min

Table 9
statistical significance testing using ANOVA.

Source of variation	Sum of Square (SS)	Degrees of Freedom (DF)	Mean Square (MS)	F-Statics	P-value
Between Groups	345.67	3	115.23	7.06	0.0003
within Groups total	153.32	20	7.67	—	—
	499.00	23	—	—	—

degrees of freedom, has a sum of squares (SS) of 345.67, resulting mean square of 115.23. The variability within groups, with 20 degrees of freedom, has an SS of 153.32, leading to an MS of 7.67. The computed F-statistic is 7.06, and the low p-value of 0.0003 indicates a statistically difference amongst the groups. In other words, there is greater variation among the groups than expected by chance alone, suggesting that the independent variable under investigation significantly impacts the dependent variable for lung cancer classification.

Table 10 shows the benchmark table using existing methods. The proposed RDCNN-TriHom-Net-WHOA-ALCD method performs better on every metric. It attains a remarkable 99.58 % accuracy, 98.37 % recall, and 98.11 % F1-score. High precision is further indicated by the low

logarithmic loss of 0.24 % and MAE of 0.18 %. The greater agreement between the predictions and ground truth is indicated by the Dice Similarity Index of 0.96 %. This thorough assessment demonstrates the proposed model's outstanding lung cancer categorization in CT images.

4.3. Discussion

In this section, the RDCNN-TriHorn-Net-WHOA-ALCD method is discussed. To improve CT image analysis, the proposed RDCNN-TriHorn-Net-WHOA-ALCD method for lung cancer detection makes use of optimal preprocessing and classification techniques. The input images are segmented using AW-BMVC and noise reduced using SAKTMF. Spectral characteristics are extracted by SOSWT, and RDCNN models are used for classification in three different strategies: RDCNN-TriHorn-Net with WHOA, RDCNN-ResNeXt-50 with AEALOA, and RDCNN-CoAtNet with DTOA. The technique detects lung cancer types such as large cell carcinoma, Adenocarcinoma, and squamous cell carcinoma with exceptional classification performance. It provides better logarithmic loss scores and dice similarity coefficients than current methods. The performance of developed RDCNN-TriHorn-Net-WHOA-ALCD model was assessed using the following metrics: accuracy, specificity, sensitivity, ROC, computation time, F1-score and precision. It has achieved dice similarity coefficient of 0.96 %, accuracy of 99.58 %, Logarithmic loss of 0.24 %, recall of 98.37 %, F1-score of 97.11 %, MAE of 0.18 %, error rate of 0.42 % by using chest CT scan images dataset and it has achieved precision of 98.56 % dice similarity coefficient of 0.96 %, accuracy of 99.58 %, Logarithmic loss of 0.24 % by using formatted and augmented chest CT scan images dataset. When compared to other existing methods such as ALCD-IDNN-CTI, CLC-SNN-CTI and RC-DNN-LNC, the proposed RDCNN-TriHorn-Net-WHOA-ALCD method shows superior performance. The proposed RDCNN-TriHorn-Net-WHOA-ALCD system surpasses existing approaches for CT image categorisation. It achieves greater accuracy, precision, and sensitivity while requiring less processing time.

5. Conclusion

The proposed RDCNN-TriHorn-Net-WHOA-ALCD approach outperforms current methods in terms of segmentation and classification accuracy, showing notable gains in lung cancer identification from CT scans. The technology successfully tackles issues like noise reduction, complex nodule formations, and low-quality CT images by applying sophisticated preprocessing, segmentation, and feature extraction algorithms. The encouraging outcomes obtained from a variety of approaches point to its potential to improve lung cancer patients' treatment outcomes and early identification. The proposed method is implemented in python. The RDCNN-TriHorn-Net-WHOA-ALCD approach attains 21.36 %, 22.45 % and 28.67 % higher F1-score, 25.01 %, 26.55 %, 27.22 % better specificity when analyzed with the existing ALCD-IDNN-CTI, CLC-SNN-CTI and RC-DNN-LNC respectively. The intrinsic heterogeneity in tumor appearance, size, and location is a

Table 10
Benchmark Table using existing methods.

Authors & Year	Accuracy (%)	Recall (%)	F1-score (%)	MAE (%)	Dice Similarity Index (%)	Logarithmic loss (%)	Error rate (%)
Shakeel et al., (2022)	82.5	75.43	68.22	0.58	0.88	0.77	17.5
(BR et al., 2024)	78.2	78.24	78.34	0.88	0.72	0.84	21.8
Chen et al., (2021)	84.70	84.70	80.34	0.71	0.68	0.89	15.3
Venkatesh et al., (2024)	85.2	85.45	83.45	0.58	0.69	0.79	14.8
Wankhade and Vigneshwari, (2023)	86.15	80.34	88.67	0.87	0.85	0.66	13.85
Saha et al., (2024)	88.45	77.33	87.29	0.70	0.79	0.73	11.55
Shashikala et al., (2024)	92.34	80.28	90.11	0.80	0.76	0.85	7.66
RDCNN-TriHorn-Net-WHOA-ALCD (proposed)	99.58	98.37	98.11	0.18	0.96	0.24	0.42

major theoretical barrier in the categorization of lung cancer using CT scan images. This variability might result in inconsistent model training. Furthermore, model accuracy and generalization may be hampered by the difficulty of integrating multi-modal information and the availability of high-quality labeled data. To overcome this limitation, future research could concentrate on refining the RDCNN-TriHorn-Net-WHOA-ALCD approach for real-time clinical use, extending its applicability to other cancer types, incorporating more imaging modalities, and enhancing algorithm efficiency and generalization across various, multi-center datasets. The RDCNN system will be extended in future work to assess its effectiveness across methods by merging WHOA, AEALOA, and DTOA optimisers with TriHorn-Net, ResNeXt-50, and CoAtNet. This will make it possible to conduct a thorough examination of accuracy, robustness, and adaptability, which will make it easier to determine the best method for detecting lung cancer.

Declaration of competing interest

The authors declare that they have no known competing financial interests or personal relationships that could have appeared to influence the work reported in this paper.

Ethical Approval and Consent to participate

This article does not contain any studies with human participants performed by any of the authors.

Human and Animal Ethics

Not Applicable.

Consent for publication

Not Applicable.

Materials and Methods

Not applicable.

Results and Discussions

Not applicable.

Declarations

Not applicable.

Funding

This research did not receive any specific grant from funding agencies in the public, commercial, or not-for-profit sectors.

Not applicable

Data availability

Data sharing does not apply to this article as no new data has been created or analyzed in this study.

References

- Abdelhamid, A. A., El-Kenawy, E. S. M., Ibrahim, A., Eid, M. M., Khafaga, D. S., Alhussan, A. A., Mirjalili, S., Khodadadi, N., Lim, W. H., & Shams, M. Y. (2023). Innovative feature selection method based on hybrid sine cosine and dipper throtted optimization algorithms. *IEEE Access*, 11, 79750–79776.
- An, J., Wang, Y., Cai, Q., Zhao, G., Dooper, S., Litjens, G., & Gao, Z. (2024). Transformer-Based Weakly Supervised Learning for Whole Slide Lung Cancer Image Classification. *IEEE J. Biomed. Health Inform.*
- Ashwini, S., Arunkumar, J. R., Prabu, R. T., Singh, N. H., & Singh, N. P. (2024). Diagnosis and multi-classification of lung diseases in CXR images using optimized deep convolutional neural network. *Soft. Comput.*, 28(7), 6219–6233.
- Barbouchi, K., El Hamdi, D., Elouedi, I., Aicha, T. B., Echi, A. K., & Slim, I. (2023). A transformer-based deep neural network for detection and classification of lung cancer via PET/CT images. *Int. J. Imaging Syst. Technol.*, 33(4), 1383–1395.
- BR, S.R.R., Sen, S., Bhatt, R., Dhanetwal, M.L., Sharma, M. & Naaz, R., (2024). Stacked neural nets for increased accuracy on classification on lung cancer. *Measurement: Sensors*, 32, p.101052.
- Chen, Y., Wang, Y., Hu, F., Feng, L., Zhou, T., & Zheng, C. (2021). LDNNET: Towards robust classification of lung nodule and cancer using lung dense neural network. *IEEE Access*, 9, 50301–50320.
- Chung, J. H., Park, J. M., & Kim, D. H. (2024). Automated CT quantification of interstitial lung abnormality in patients with resectable stage I non-small cell lung cancer: Prognostic significance. *Thoracic. Cancer*.
- Han, B., Zhou, Y., & Yu, G. (2021). Second-order synchroextracting wavelet transform for nonstationary signal analysis of rotating machinery. *Signal Process.*, 186, Article 108123.
- Houfar, K., Samai, D., Dornaika, F., Benlamoudi, A., Bensid, K., & Taleb-Ahmed, A. (2023). Automatically weighted binary multi-view clustering via deep initialization (AW-BMVC). *Pattern Recogn.*, 137, Article 109281.
- <https://www.kaggle.com/datasets/addislissan/chest-ct-scan-images-dataset>.
- <https://www.kaggle.com/datasets/benjaminmaizes/formatted-and-augmented-chest-ct-scan-images/data>.
- Imran, M., Haq, B., Elbasi, E., Topcu, A. E., & Shao, W. (2024). Transformer Based Hierarchical Model for Non-Small Cell Lung Cancer Detection and Classification. *IEEE Access*.
- Kumar, A., Mehta, R., Reddy, B. R., & Singh, K. K. (2024). Vision Transformer Based Effective Model for Early Detection and Classification of Lung Cancer. *SN Comput. Sci.*, 5(7), 839.
- Lin, C. Y., Guo, S. M., Lien, J. J. J., Tsai, T. Y., Liu, Y. S., Lai, C. H., Hsu, I. L., Chang, C. C., & Tseng, Y. L. (2024). Development of a modified 3D region proposal network for lung nodule detection in computed tomography scans: A secondary analysis of lung nodule datasets. *Cancer Imaging*, 24(1), 40.
- Murthy, S. V. S. N., & Prasad, P. M. K. (2023). Adversarial transformer network for classification of lung cancer disease from CT scan images. *Biomed. Signal Process. Control*, 86, Article 105327.
- Nagarathna, C. R., & Chinnaswamy, C. N. (2014). The technique to detect and avoid the denial of service attacks in wireless sensor networks. *International Journal of Research in Engineering and Technology (IJRET)*, 3(05).
- Nagarathna, C. R., & Kusuma, M. (2021, November). Comparative study of detection and classification of Alzheimer's disease using Hybrid model and CNN. In , 1, 2021 International Conference on Disruptive Technologies for Multi-Disciplinary Research and Applications (CENTCON) (pp. 43–46). IEEE.
- Nagarathna, C. R., & Kusuma, M. (2022). Automatic Diagnosis of Alzheimer's disease using Hybrid Model and CNN. *Journal of Soft Computing Paradigm*, 3(4), 322–335.
- Nissar, A., & Mir, A. H. (2024). Proficiency evaluation of shape and WPT radiomics based on machine learning for CT lung cancer prognosis. *Egypt. J. Radiol. Nucl. Med.*, 55(1), 50.
- Panneer, K. S. V., & Jaganathan, K. (2024). Adaptive Elite Ant Lion Optimizer tuned optimal controller for underactuated systems. *Franklin Open*, 6, Article 100085.
- Prasad, U., Chakravarty, S., & Mahto, G. (2024). Lung cancer detection and classification using deep neural network based on hybrid metaheuristic algorithm. *Soft. Comput.*, 28(15), 8579–8602.
- Priyadarshini, K., Alagarsamy, M., Sangeetha, K., & Thangaraju, D. (2024). Hybrid RNN-FFBPNN Optimized with Glowworm Swarm Algorithm for Lung Cancer Prediction. *IETE J. Res.*, 70(5), 4453–4468.
- Rezaei, M., Rastgoor, R., & Athitsos, V. (2023). TriHorn-net: A model for accurate depth-based 3D hand pose estimation. *Expert Syst. Appl.*, 223, Article 119922.
- Saha, A., Ganie, S. M., Pramanik, P. K. D., Yadav, R. K., Mallik, S., & Zhao, Z. (2024). VER-Net: A hybrid transfer learning model for lung cancer detection using CT scan images. *BMC Med. Imaging*, 24(1), 120.
- Sangeetha, S. K. B., Mathivanan, S. K., Karthikeyan, P., Rajadurai, H., Shivahare, B. D., Mallik, S., & Qin, H. (2024). An enhanced multimodal fusion deep learning neural network for lung cancer classification. *Syst. Soft Comput.*, 6, Article 200068.
- Shakeel, P. M., Burhanuddin, M. A., & Desa, M. I. (2022). Automatic lung cancer detection from CT image using improved deep neural network and ensemble classifier. *Neural Comput. & Appl.*, 1–14.
- Shao, X., Ge, X., Gao, J., Niu, R., Shi, Y., Shao, X., Jiang, Z., Li, R., & Wang, Y. (2024). Transfer learning-based PET/CT three-dimensional convolutional neural network fusion of image and clinical information for prediction of EGFR mutation in lung adenocarcinoma. *BMC Med. Imaging*, 24(1), 54.
- Shashikal, D., Chandran, C. P., & Rajathi, S. (2024). Cross-spectral vision transformer for lung nodule detection with improved moth flame algorithm using deep learning. *e-Prime-Advances in Electrical Engineering. Electronics and Energy*, 8, Article 100556.
- Subash, J., & Kalaivani, S. (2024). Dual-stage classification for lung cancer detection and staging using hybrid deep learning techniques. *Neural Comput. & Appl.*, 36(14), 8141–8161.
- Suganthy, M., Krishnamoorthy, R., Nagarajaiah, K., & DayaSagar, K. V. (2024). Lung Cancer Classification based on Auxiliary Classifier (WGAN) Optimised with HOA from CT Images. *IETE J. Res.*, 1–9.
- Tripathi, S., Augustin, A. I., Sukumaran, R., Dheer, S., & Kim, E. (2022). HematoNet: Expert level classification of bone marrow cytology morphology in hematological malignancy with deep learning. *Artif. Intell. Life Sci.*, 2, Article 100043.
- Vasantrao, C. P., & Gupta, N. (2023). Wader hunt optimization based UNET model for change detection in satellite images. *Int. J. Inf. Technol.*, 15(3), 1611–1623.

- Venkatesan, N., Pasupathy, S., & Gobinathan, B. (2024). An efficient lung cancer detection using optimal SVM and improved weight based beetle swarm optimization. *Biomed. Signal Process. Control*, 88, Article 105373.
- Venkatesh, C., Chinnababu, J., Kiran, A., Nagaraju, C. H., & Kumar, M. (2024). A hybrid model for lung cancer prediction using patch processing and deeplearning on CT images. *Multimed. Tools Appl.*, 83(15), 43931–43952.
- Wani, N. A., Kumar, R., & Bedi, J. (2024). DeepExplainer: An interpretable deep learning based approach for lung cancer detection using explainable artificial intelligence. *Comput. Methods Programs Biomed.*, 243, Article 107879.
- Wankhade, S., & Vigneshwari, S. (2023). A novel hybrid deep learning method for early detection of lung cancer using neural networks. *Healthcare Anal.*, 3, Article 100195.
- Yoo, S. J., Park, Y. S., Choi, H., Kim, D. S., Goo, J. M., & Yoon, S. H. (2024). Prospective evaluation of deep learning image reconstruction for Lung-RADS and automatic nodule volumetry on ultralow-dose chest CT. *PLoS One*, 19(2), Article e0297390.
- Zhan, M., Zhao, C., Qin, K., Huang, P., Fang, M., & Zhao, C. (2023). Subaperture keystone transform matched filtering algorithm and its application for air moving target detection in an SBEWR system. *IEEE Journal of Selected Topics in Applied Earth Observations and Remote Sensing*, 16, 2262–2274.
- Zhang, F., Wang, Q., Fan, E., Lu, N., Chen, D., Jiang, H., & Yu, Y. (2024). Enhancing non-small cell lung cancer tumor segmentation with a novel two-step deep learning approach. *J. Radiat. Res. Appl. Sci.*, 17(1), Article 100775.
- Zhang, Q., Xiao, J., Tian, C., Chun-Wei Lin, J., & Zhang, S. (2023). A robust deformed convolutional neural network (CNN) for image denoising. *CAAI Trans. Intell. Technol.*, 8(2), 331–342.